Alternative characterization of the nematic transition in deposition of rods on two-dimensional lattices

E. E. Vogel,[1,2] G. Saravia,[1] A. J. Ramirez-Pastor,[3] and Marcelo Pasinetti[3,*]
[1]Departamento de Ciencias Físicas, CEMCC, Universidad de La Frontera, Casilla 54-D, Temuco, Chile
[2]Center for the Development of Nanoscience and Nanotechnology (CEDENNA), 9170124 Santiago, Chile
[3]Departamento de Física, Instituto de Física Aplicada (INFAP), Universidad Nacional de San Luis - CONICET, Ejército de Los Andes 950, D5700HHW San Luis, Argentina

(Received 7 October 2019; revised manuscript received 23 November 2019; accepted 23 December 2019; published xxxxxx)

We revisit the problem of excluded volume deposition of rigid rods of length k unit cells over square lattices. Two new features are introduced: (a) two new short-distance complementary order parameters, called Π and Σ, are defined, calculated, and discussed to deal with the phases present as coverage increases; (b) the interpretation is now done beginning at the high-coverage ordered phase which allows us to interpret the low-coverage nematic phase as an ergodicity breakdown present only when $k \geqslant 7$. In addition the data analysis invokes both mutability (dynamical information theory method) and Shannon entropy (static distribution analysis) to further characterize the phases of the system. Moreover, mutability and Shannon entropy are compared, and we report the advantages and disadvantages they present for their use in this problem.

DOI: 10.1103/PhysRevE.00.002100

I. INTRODUCTION

The study of systems of hard rod-like particles having different geometrical shapes has been of continued interest in classical statistical mechanics. A pioneer contribution to this subject was made by Onsager [1], who predicted that very long and thin rods interacting by means of excluded-volume interaction only can lead to long-range orientational (nematic) order. This nematic phase, characterized by a big domain of parallel molecules, is separated from an isotropic state by a phase transition occurring at a finite critical density.

The phase properties of systems with purely steric interactions are important from a statistical mechanical perspective because temperature plays no role, and all phase transitions are entropy driven. The problem proposed by Onsager is a clear example of an entropy-driven phase transition. Other examples, corresponding to phase transitions in systems of hard particles of different shapes include triangles [2], squares [3–9], dimers [10–13], mixtures of squares and dimers [14,15], Y-shaped particles [16–18], tetrominoes [19,20], rods [21–36], rectangles [26,37–39], disks [40,41], and hexagons [42]. Experimental realizations of such systems include tobacco mosaic virus [43,44], liquid crystals [45], fd virus [46–48], silica colloids [49,50], boehmite particles [51,52], DNA origami nanoneedles [53], as well as simple models for studying adsorption of molecules onto two-dimensional (2D) substrates [54–56].

For the continuum problem, there is general agreement that in the case of deposition of infinitely thin rods in three dimensions the system undergoes a first-order phase transition [1]. On the other hand, in two dimensions, when the rods may orient in any direction, the continuous rotational symmetry remains unbroken at any density. However, the system undergoes a Kosterlitz-Thouless-type transition from a low-density phase with exponential decay of orientational correlations to a high-density phase with a power-law decay [57–60].

The lattice version of the problem, which is the topic of this paper, has also been studied in the literature. Here, the hard rods are composed of k collinear and consecutive sites of a regular lattice (k-mers). No two k-mers are allowed to intersect, and all allowed configurations have the same energy. Ghosh and Dhar [21] investigated the problem on square lattices. Using Monte Carlo (MC) simulations and analytical arguments based on the classical orientational order parameter (designated as δ below), the authors found that the deposition of straight rods presents no special characteristics until the length of the rod is 7 times the lattice constant. From there up, ordering appears and two transitions were reported as function of the coverage θ (fraction of the occupied sites): first, at $\theta = \theta_1$, from a low-density disordered to an intermediate-density nematic phase and second, at $\theta = \theta_2$, from the nematic to a high-density disordered phase.

Later, and based on the seminal work of Ghosh and Dhar [21], several papers were devoted to the detailed study of the transition occurring at intermediate density values in a system of long straight rigid rods on 2D lattices with discrete allowed orientations [22–29]. This transition was usually referred to as isotropic to nematic (I-N) but due to the results presented below the high coverage phase is also isotropic but ordered, while the low-density isotropic phase is disordered. We propose referring to these phases as disordered-isotropic (D), nematic (N), and ordered-isotropic (O) in the order they appear when coverage is increased.

*pmp@unsl.edu.ar

In the just cited articles, it was shown that (1) the D-N phase transition belongs to the 2D Ising universality class for square lattices and the three-state Potts universality class for honeycomb and triangular lattices [22,23]; (2) the critical value of k which allows the formation of a nematic phase is $k = 7$ for square and triangular lattices [22,24] and $k = 11$ for honeycomb lattices [23]; (3) the critical density characterizing the D-N transition θ_1 follows a power law as $\theta_1(k) \propto k^{-1}$ [24–26]; and (4) the orientational order survives in a wide range of lateral interactions between the adsorbed k-mers [27–29].

The study of the second transition (N-O) using simulations is more difficult due to the presence of many long-lived metastable states. Conventional MC algorithms using deposition-evaporation moves involving only addition or removal of single rods at a time are quite inefficient at large densities. For these reasons, there have been few studies related to the second transition from the nematic phase to the high-density phase [30–32]. However, this transition is the most essential issue in the present article as the high coverage phase is present for all systems regardless of the k value, as will be shown below.

In Ref. [21], Ghosh and Dhar found that $\theta_2 \approx 1 - Ck^{-2}$ for large values of k, where C is some constant. Linares *et al.* [30] provided numerical evidence for the existence of the N-O phase transition at high coverage. The case of linear 7-mers ($k = 7$) on square lattices was studied and the corresponding critical density was estimated to be between 0.87 and 0.93. On the other hand, using an efficient grand-canonical MC algorithm, Kundu *et al.* [31,32] studied the problem of straight rigid rods on square and triangular lattices at densities close to full packing. However, the nature of the second transition from the nematic phase to the high-density phase, that is neither nematic or disordered, is still an open problem.

On square lattices, the second transition is continuous with effective critical exponents that are different from the 2D Ising exponents [32]. On triangular lattices the critical exponents are numerically close to those of the first transition [32]. This raises the question whether the low-density disordered and high-density disordered phases are the same or they correspond to different phases. If this is the case, the order parameter δ designed to recognize the low coverage phase transition does not necessarily properly characterizes this high coverage phase transition. This is the reason we search for new ways to better characterize this high-coverage phase upon defining two different local-order parameters intended to recognize local order.

From a theoretical point of view, rigorous results are still very limited. In this line, Heilmann and Lieb [12] showed that, for $k = 2$, the system is disordered at all densities. The existence of the intermediate nematic phase, and hence the D-N phase transition, has been rigorously proved [33]. The problem of hard rods was solved exactly on a Bethe-like lattice [34,35]. The solution obtained leads to continuous or discontinuous isotropic-nematic transitions for sufficiently high values of k, depending of the coordination number of the lattice. The second transition does not occur on such a lattice [34], although two transitions are found on a Bethe-like lattice if additional repulsive interactions between the rods are included [35].

The behavior of long rods has also been studied by using approximate methods [61,62]. Based on the configuration-counting procedure of the Guggenheim approximation [63], DiMarzio [61] showed the existence of nematic order in a lattice model of straight rigid rods. Identical results were obtained in Ref. [62], by using density functional theory.

In a recent paper from our group, an alternative numerical method to treat orientational phase transitions was applied to the hard-rod problem on square lattices [36]. The approach is based on the application of information theory using data compressor WLZIP for the recognition of repetitive data in time series such as those generated in Monte Carlo simulations of magnetic systems [64–66]. The method was then applied to recognize volatility and critical periods in stock markets [67] and pension funds [68]. The time series obtained from ambulatory measurement of blood pressure also can be analyzed by means of this information theory technique, allowing one to characterize vascular risk [69]. The information recognition focused next on the time series associated with the intervals between consecutive seisms, finding an indicator that increases several months before a major earthquake [70]. More recently the same technique was applied to wind energy production, finding favorable periods for the use of this technology thus saving fuels [71].

Shannon entropy is a better known data analyzer [72]. It is based on the probability of visiting a state characterized by the value of a given parameter regardless of the time sequence in which the visits took place. Hence it is the only static measure of a given distribution in contrast to mutability that can produce different results depending on the order the visits took place. In any case, Shannon entropy has been used to study a variety of nonlinear dynamical phenomena such as magnetic transitions, the Rayleigh-Bernard convection, the 3D magnetohydrodynamics model of plasmas, and turbulence or time series produced by seismic activity [73–78].

Besides applying these two numerical techniques to the problem, we shall discuss their similarities and differences in practical terms. We will end up preferring mutability for the present transitions and we will justify this choice.

This paper is organized as follows: the model, simulation scheme, and basic definitions are given in Sec. II; there, the order parameters are defined and the measurement methods, mutability and Shannon entropy, are reviewed. Section III is devoted to the main results of the application of the new technique and the comparison with previous results. Finally, the general conclusions are given in Sec. IV.

II. MODEL AND SIMULATION SCHEME

A. Deposition dynamics

Straight rigid rods containing k identical constituents (k-mers) are deposited on a perfect match on square lattices. Namely, the distance between k-mer units is equal to the lattice constant, so exactly k sites are occupied by a k-mer deposition; the width of the k-mer is one lattice constant. No other interactions than hard-core exclusion are present: no site can be occupied by more than one k-mer unit. The substrate is represented as an array of $M = L \times L$ sites; conventional periodic boundary conditions are imposed.

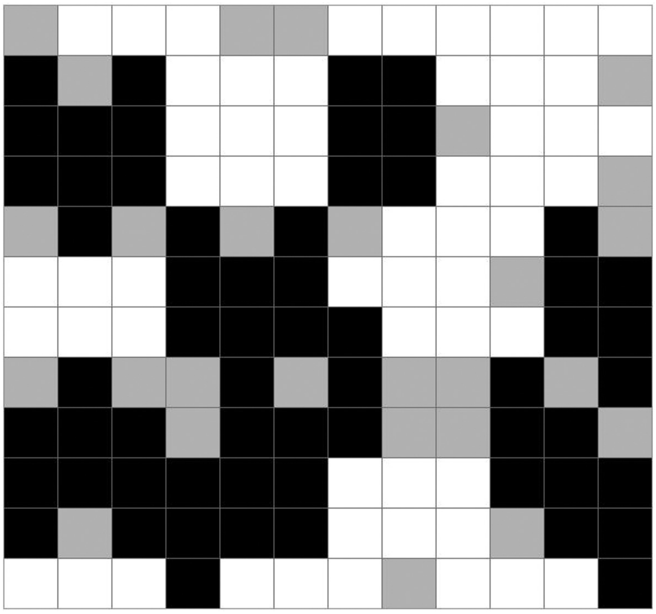

FIG. 1. Example of a saturated deposition (jamming condition) of liner trimers ($k = 3$) for a density $\theta = 0.8125$ on a square lattice with $L = 12$. Horizontal trimers are painted white, vertical trimers are painted black, and empty sites are painted gray.

MC simulations were carried out in the grand-canonical ensemble where temperature T, system size L, and chemical potential μ are held fixed while the number of adsorbed particles (linear k-mers or rods) is allowed to fluctuate. To overcome the slowdown in the configuration sampling at high densities due to jamming effects, we use an efficient algorithm introduced by Kundu *et al.* [31,32]. This algorithm, in contrast to the standard Metropolis algorithm [79], makes nonlocal changes, i.e., adsorption or desorption of many particles at a time, so that it is possible to sample at equilibrium configurations of density near unity in an effective way. The process begins by distinguishing horizontal from vertical k-mers, naming them x-mers and y-mers. Then, starting with the horizontal direction, all the x-mers in the system are evaporated. Each row now consists of sets of contiguous empty sites, separated from each other by sites occupied by y-mers. Thus, the system can be seen as a collection of horizontal spaces of length l ($\leqslant L$). The lattice is now reoccupied with x-mers. This reduces the problem to the 1D problem of filling each space of length l with particles of length k (x-mers) with equilibrium configurations. Finally, the same process is repeated for the vertical direction, completing the elementary MC step (1 MCS) of the algorithm.

The algorithm has been proved to be ergodic [31,32] and allowed us to reach equilibrium in reasonable time for the different conditions present in this study. This is usually achieved after discarding $n_0 = 10^7$ MCS, and then the different observables are averaged throughout the next $n_1 = 10^7$ MCS. Additionally, L/k values up to 80 were considered to ensure finite size effects are negligible. The results showed that, for most of the cases, values around $L/k = 10$ yielded results similar to those of systems with larger ratios; this is important since these small L/k systems are less expensive in terms of computational cost.

Figure 1 shows the trimer ($k = 3$) deposition on a 12×12 lattice. To guide the eye the 19 horizontal trimers are painted white while the 20 vertical trimers are painted black, although there is no probabilistic distinction between these two kind of depositions. The 27 empty spaces are painted gray. Thus, the density or coverage for this example is

$$\theta = \frac{kN}{M} = \frac{117}{144} = 0.8125, \tag{1}$$

where N is the total number of k-mers adsorbed on the lattice. In the MC simulations, the chemical potential is varied while the density is monitored.

B. Order parameters

The standard order parameter to deal with this problem for square lattices is defined as [21,22,80]

$$\delta = \frac{|n_1 - n_2|}{(n_1 + n_2)}, \tag{2}$$

where n_1 (n_2) is the number of k-mers aligned along the horizontal (vertical) direction.

For the example given in Fig. 1 this order parameter can be readily calculated,

$$\delta = \frac{|19 - 20|}{(19 + 20)} = 0.026, \tag{3}$$

indicating that essentially there is no preferred deposition direction.

However this parameter does not consider other forms of possible ordering, for instance local arrangements of k-mers forming patches like intercalated paths or chessboard-like patterns (see Fig. 2) which can lead to a very small δ value but indicating a local correlation. To cope with this possibility we will construct here a simple algebra which will allow us to define two new order parameters.

First, let us assign labels to each position (i, j) in the lattice of Fig. 1: i runs over the columns from left to right, while j runs over the rows from top to bottom. Now we assign numerical values to the lattice sites thus defining a matrix $m(i, j)$ with the occupied and empty sites: empty (gray) site is zero, any site belonging to a horizontal rod (white) is $+1$, any site belonging to a vertical rod (black) is -1. Thus, the second row in the example, $m(i, 2)$, would be $-1, 0, -1, +1, +1, +1, -1, -1, +1, +1, +1, 0$, where we have used commas to separate the positions from $m(1, 2)$ to $m(12, 2)$.

The quantity $m(i, j)$ was previously defined and used by Kundu *et al.* [32] to calculate the order parameter correlation function, C_{SS}, as a function of the distance between two lattice sites r. In Ref. [32], the authors showed that $C_{SS}(r)$ has an oscillatory dependence on distance with period k, and for $r \gg k$ appears to decrease as a power law $r^{-\eta}$, with $\eta > 2$.

In the present contribution, $m(i, j)$ will be used in a different and complementary way, namely, to build two new order parameters destined to characterize the critical behavior of the system. For this purpose, we start by defining the directional products between two neighboring sites. The horizontal product associated to site (i, j) is defined as

$$h(i, j) = +1 \tag{4}$$

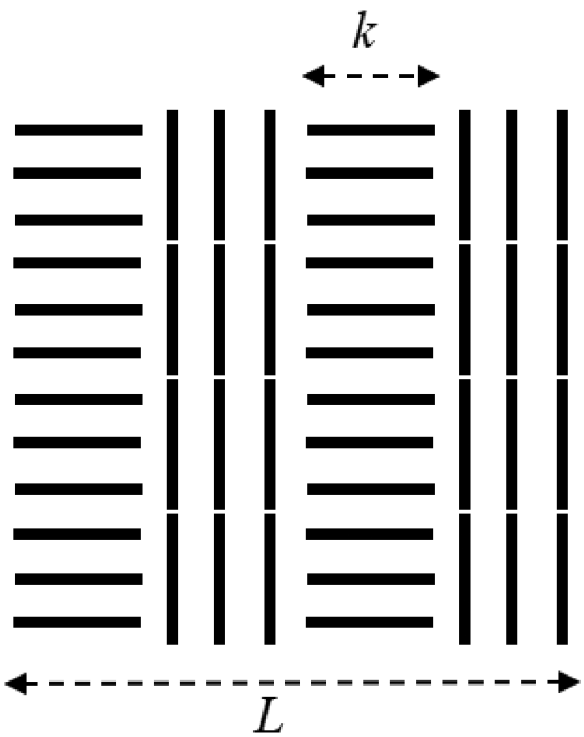

FIG. 2. Optimized path-like deposition of rods of length k on an $L \times L$ square lattice under commensurate conditions. Proportions here are for $L = 12$ and $k = 3$.

if both $m(i, j)$ and $m(i + 1, j)$ take the value -1, while

$$h(i, j) = 0 \tag{5}$$

otherwise.

On the other hand the vertical product associated to the position (i, j) is defined as

$$v(i, j) = +1 \tag{6}$$

if both $m(i, j)$ and $m(i, j + 1)$ take the value $+1$, while

$$v(i, j) = 0 \tag{7}$$

otherwise.

Periodic boundary conditions are imposed to previous algebra. We now add the products along columns and rows to define directional indicators in the following way:

$$\sigma_h = \frac{1}{M} \sum_{j=1}^{L} \sum_{i=1}^{L} h(i, j) \tag{8}$$

and

$$\sigma_v = \frac{1}{M} \sum_{i=1}^{L} \sum_{j=1}^{L} v(i, j). \tag{9}$$

For the example given in Fig. 1 we readily obtain $\sigma_h = 32/144$ and $\sigma_v = 34/144$.

With these indicators we can now define two parameters, Σ and Π:

$$\Sigma = \frac{\sigma_h + \sigma_v}{R_S(L, k)}, \tag{10}$$

$$\Pi = \frac{\sigma_h * \sigma_v}{R_P(L, k)}. \tag{11}$$

The divisors $R_S(L, k)$ and $R_P(L, k)$ represent the normalization factors for Σ and Π respectively. They are obtained from previous equations for an arbitrary saturation configuration; we choose the one presented in Fig. 2 for the particular case of $L = 12$, $k = 3$. For perfectly commensurate lattices ($L = f \times k$, with f an integer number) the optimized stripes distribution leads to

$$R_S(L, k) = 1 - \frac{1}{2k} \tag{12}$$

and

$$R_P(L, k) = \frac{1}{4}\left(1 - \frac{1}{k}\right). \tag{13}$$

It is very interesting that for this particular configuration the normalization factors are independent of L, which is an advantage for comparison purposes among different lattice sizes. For the example given in Fig. 2 we get $R_S(12, 3) = 0.8333$ and $R_P(12, 3) = 0.1667$.

C. Information content and Shannon entropy

A useful measure of the information content of any sequence is the mutability ζ, whose definition we review next. Let $w(Q, \nu, t)$ be the weight in bytes of the vector file $Q(\nu, t)$ storing the sequence of parameter Q along ν episodes labeled by symbol t (it could be any kind of ordered information). Then, this file is processed by data compressor WLZIP [65–67] yielding a new file whose weight in bytes is $w^*(Q, \nu)$, where the original order is hidden within the map created by WLZIP. It should be noticed that no information has been lost since the inverse algorithm can be invoked to restore the original file $Q(\nu, t)$, although this process will not be necessary here. Then, the mutability associated with the sequence of parameter $Q(\nu, t)$ is given by the ratio

$$\zeta(Q, \nu) = \frac{w^*(Q, \nu)}{w(Q, \nu, t)}. \tag{14}$$

This procedure was already applied to order parameter δ [36], where more details about the procedure can be found. In the present article we shall apply WLZIP to parameters Σ and Π for k in the range ($3 \leqslant k \leqslant 11$) and $L/k = 10$ (in some selected cases, higher values of L/k were considered to test the stability).

A better known similar parameter is the Shannon entropy associated with $Q(\nu, t)$, which is defined as

$$H(\nu, t) = -\sum_{j=}^{\nu} p_j \ln(p_j), \tag{15}$$

where p_j is the probability distribution function of finding the value $Q(\nu, t_j)$ in the ν instants previous to time t; if such value is found g_j times in the sequence of ν measurements the probability p_j is simply given by

$$p_j = g_j/\nu. \tag{16}$$

We shall use the same dynamic time window ν for the evaluation of both mutability and Shannon entropy to allow for comparison. It turns out that it is the former that produces sharper curves, pointing to better resolved maximum values,

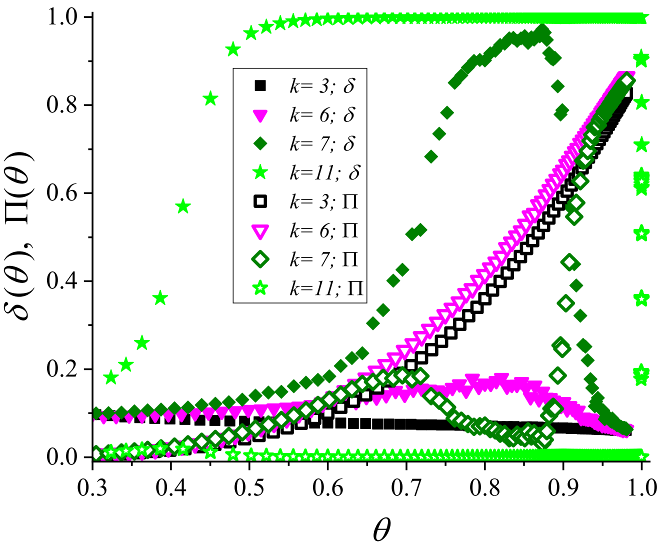

FIG. 3. Classical parameter δ (filled symbols) and new parameter Π (hollow symbols) as functions of the deposition density θ for selected k values 3, 6, 7, 11, using lattices with $L = 10k$.

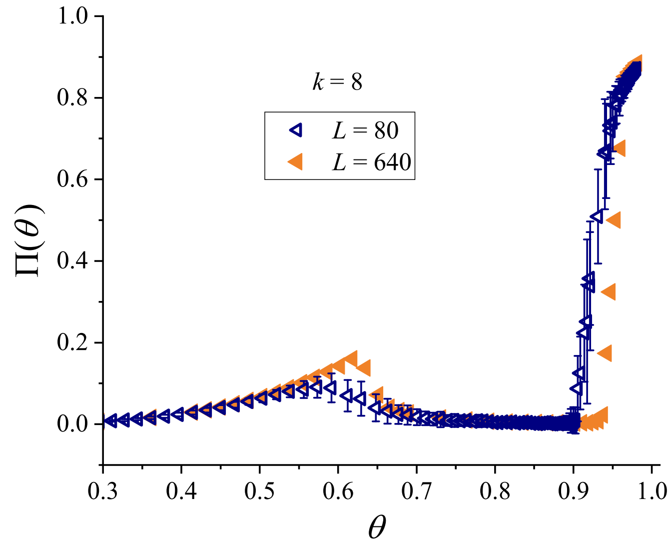

FIG. 4. Parameter $\Pi(\theta)$ for $k = 8$ deposited on lattices of two very different sizes: $L = 10k$ and $L = 80k$.

so we will show mutability values most of the time, illustrating Shannon entropy in just one case.

III. RESULTS AND DISCUSSION

To avoid overcrowding in the following figures, we present curves for selected k values, varying them through the different figures in the range ($3 \leqslant k \leqslant 11$). The reason to stop at $k = 11$ is exclusively due to the huge computer times involved for larger k values, as will be discussed towards the end of the present section. Symbol shapes (and color when available) are kept the same for each k value through the pertinent figures.

Parameter $\Pi(\theta)$ will turn out to better describe all the stages or phases of the system for different values of k as the deposition density θ increases. So we begin by comparing the behavior of this parameter with the classical parameter δ, which is done in Fig. 3. As can be seen, δ is low for $k = 3$ and 6, while it rises to unity for $k = 7$ and 11, thus evidencing the nematic transition for $k \geqslant 7$. Actually, a closer observation reveals that, for $k = 6$, δ tends to depart from very low values, while for $k = 7$ unity is not quite reached. Then the limiting behavior for the nematic transition is clearly between these two values of k. This is the expected behavior of this parameter used here for comparison purposes [36]. On the other hand, parameter $\Pi(\theta)$ shows a monotonic and almost coincidental behavior for $k = 3$ and 6, but it presents a clear structure for the higher values of k, which we discuss separately.

For $k = 7$ parameter $\Pi(\theta)$ maximizes just under $\theta = 0.7$, coinciding with the inflection point of $\delta(\theta)$ precisely at this point; so the onset of the nematic transition is recognized by both parameters. Then $\Pi(\theta)$ begins to rise precisely at the concentration where δ begins its descent, evidencing that the nematic ordering is lost but without pointing to any characteristic of the emerging phase. However, $\Pi(\theta)$ continues to increase, evidencing that the order that was built into its definition is establishing. This is the short-order nematic phase in the form of paths of width nearly or just over k. Surprisingly $\Pi(\theta)$ recognizes both transitions, although the low coverage transition was not intended.

For $k = 11$ the situation is the same as that for $k = 7$ except that transitions are more abruptly obtained. Thus $\Pi(\theta)$ presents a maximum just over $\theta = 0.4$ at the inflection point of $\delta(\theta)$. Although this maximum is barely visible in this scale it is very well defined when a more appropriate scale is used. Then, when θ approaches the limit of high coverage, δ and Π cross each other with the former descending and the latter ascending, thus marking the appearance of the phase present at high coverage: the path-like near-distance ordering. Curves for other values of $k \geqslant 7$ present this same structure, whch will be presented in some of the following figures when discussing other properties.

Previous results were obtained for $L/k = 10$. Is it enough to use values of L of this sort to validate the phenomenon and to legitimate the new parameter Π? We did a systematic study, varying L/k from 10 to 80, finding only small changes in the value of the coverage for the maxima of $\Pi(\theta)$ but preserving the phenomenon and the tendencies. We illustrate this response in Fig. 4 for $k = 8$ using the extreme values of the range of L/k values explored, namely 10 and 80. As can be seen, the only changes are the slight shifts to higher coverage values when larger lattices are employed. Since large values of L mean huge computer times, we shall stick to $L/k = 10$ in the present paper, intending to analyze the behavior of the new parameters rather than reporting exact values for them.

Parameter $\Sigma(\theta)$ is plotted in Fig. 5 for different values of k. The main body covers values of $k = 3$, 4, 5, 6, and 7 up to $\theta = 0.8$; all curves grow monotonically, not showing the expected low coverage nematic transition for $k = 7$ near $\theta = 0.7$. The inset displays curves for $k = 6$, 7, 8, 9, and 10, over $\theta = 0.85$, where broad indications for the high coverage transitions are obtained near the expected concentrations for the different k values; the general tendency of increasing the critical coverage as k grows is also established. Evidently

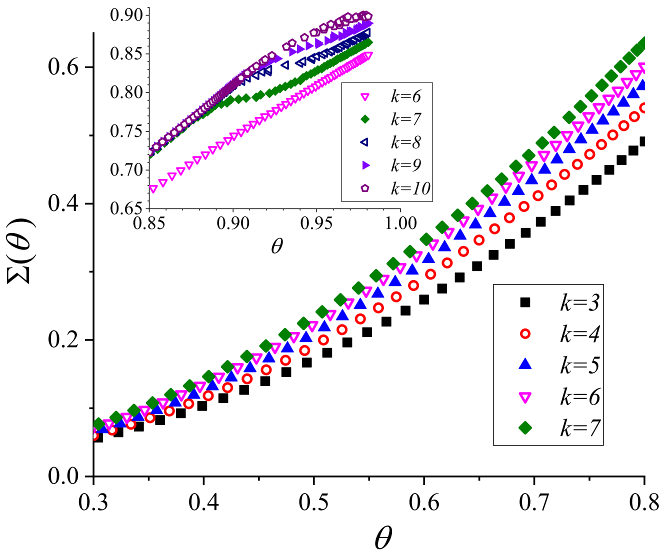

FIG. 5. Order parameter Σ as function of θ for several k values with $L/k = 10$.

parameter $\Sigma(\theta)$ does not provide significant information related to the possible phases present in the system.

We go back now to parameter $\Pi(\theta)$ to establish the different responses for low and high values of k. This is done in Fig. 6 for $k = 4, 5, 8,$ and 9, complementary to those of Fig. 3. Curves for low-k values are almost coincidental, ascending monotonically to their maximum values close to unity; no indication for any ordering appears. However, the curves for the high-k values present clear maxima at low coverage, which represents the onset of the transition to the nematic phase. The value of the maximum shifts to lower coverage, as can be expected from the results of the $\delta(\theta)$ order parameter [36]. As θ increases $\Pi(\theta)$ tends to vanish and remains near zero until at θ slightly over 0.9 it very abruptly rises, with the curve for

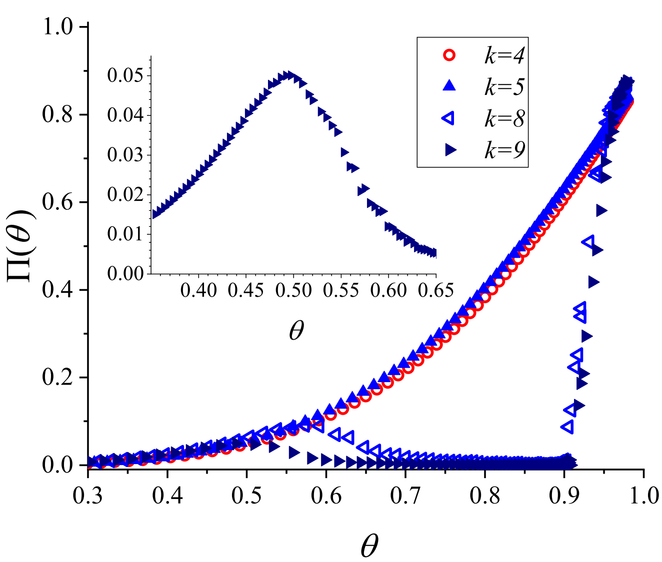

FIG. 6. Parameter Π as function of θ for $k = 4, 5, 8, 9$ and $L/k = 10$. The inset shows the minimum at lower coverage for $k = 9$ better resolved in an appropriate scale.

larger k value displaced to the right (higher coverage). This parameter is intended to recognize the path-like ordering, so the high value of this parameter indicates that this is the kind of configuration that dominates in the high coverage regime.

However, the most striking fact shown by Fig. 6 is that all curves have a common origin and a coincidental response under the low coverage maximum, and they also have a similar tendency and final values towards deposition saturation. The interpretation is clear: deposition for all k values tend to the same high coverage phase in the form of mixed horizontal and vertical paths; this tendency is interrupted for $k \geqslant 7$ where an ergodic breakdown arises favoring depositions along one of the two possible directions only. In the slow high coverage dynamics, group shifts dominate over individual rod shifts and the path-like structures are generated.

It is interesting to notice that for $3 \leqslant k \leqslant 6$ parameter $\Pi(\theta)$ reaches its maximum value softly. So the high coverage phase is reached by means of an evolutionary process without drastic changes in the properties of the system. But for $k \geqslant 7$ this evolutionary process is abruptly changed due to the surge of an ordered phase, a nematic ordering, at the concentration $\theta = \theta_1$ for the corresponding k value. This means an immediate decrease of parameter $\Pi(\theta)$ *near* θ_1 (not necessarily at the θ_1 value obtained by a different order parameter). Then, $\Pi(\theta)$ stays at values near 0.0 until the nematic order disappears and parameter $\Pi(\theta)$ recovers abruptly to the values of the interrupted monotonic increasing tendency shown by lower values of k.

The inset of Fig. 6 is intended to show that the low-coverage transition is well recognized by parameter $\Pi(\theta)$, although it can be somewhat hidden in a large scale used in the plot. The value at which $\Pi(\theta)$ maximizes is not necessarily the same as the θ_1 value found by other methods since it is measuring a different property. However, this value should follow tendencies similar to any other similar values for θ_1 as k varies.

To investigate what kind of phases and transitions are present, we prepared a succession of snapshots for $k = 5$ (D-N phase transition is not present) and for $k = 8$ (with phase transitions at θ_1 and θ_2), increasing coverage at the same steps. Results are reported in Fig. 7, where different evolution processes are observed for these two k values. In the case of $k = 5$ we find a continuous evolution towards a path-like configuration somewhat similar to the optimal one shown in Fig. 2. On the other hand, for the case of $k = 8$ we observe a clear nematic ordering over a characteristic concentration ($\theta_1 \approx 0.58$). Then, as the depositions continue, the nematic phase prevails until the concentration reaches a second characteristic concentration ($\theta_2 \approx 0.92$) when the systems abruptly tend to the short order path-like configuration present for all k values. Values for the concentration θ, order parameter $\Pi(\theta)$, and mutability ζ for parameter $\Pi(\theta)$ are given to the right of each row.

From previous discussion, we propose here that the second phase transition is nothing but the disappearance of the nematic order, followed by the recovery of the evolution towards the high-coverage configuration. To appreciate that this high concentration phase is basically independent of k, a gallery of snapshots obtained for different k is presented in Fig. 8. In all cases, the concentration is $\theta \approx 0.98$, namely, over θ_2.

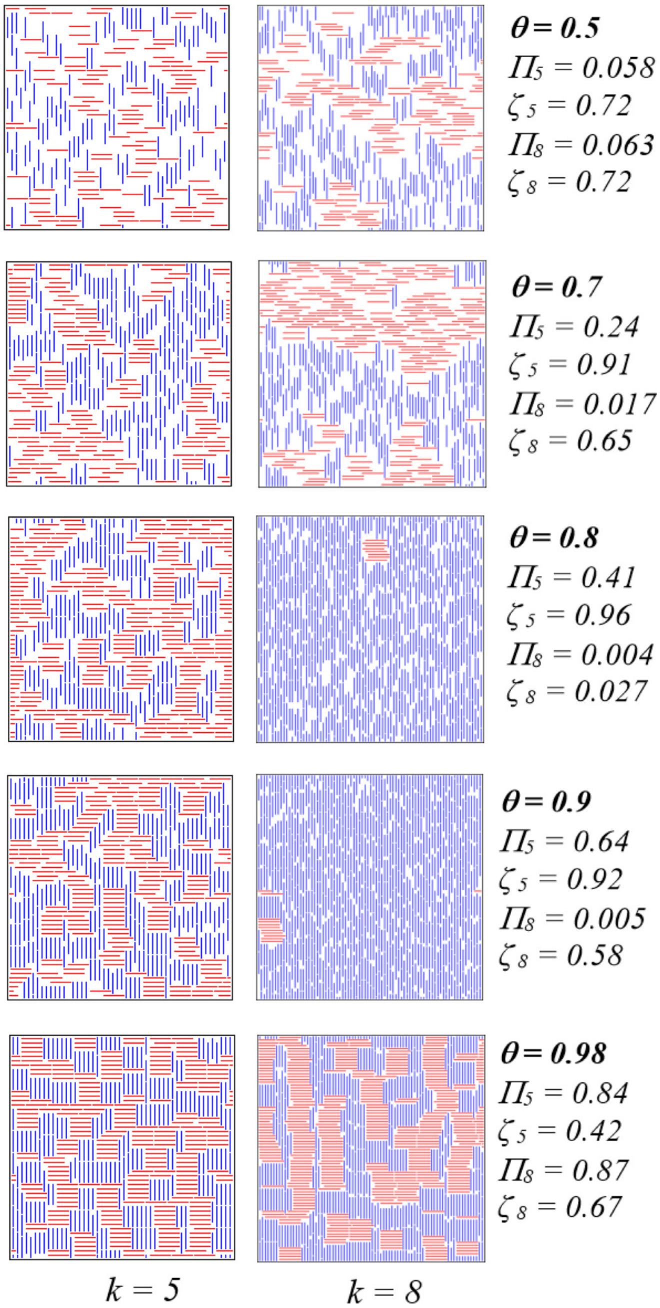

FIG. 7. For $k = 5$ (left column) and for $k = 8$ (right column) we present snapshots showing the different orderings reached as the concentration is increased from top to bottom. The corresponding values of the concentration θ and parameters $\Pi_k(\theta)$ and $\zeta(\Pi_k(\theta))$ are given to the right of the pictures.

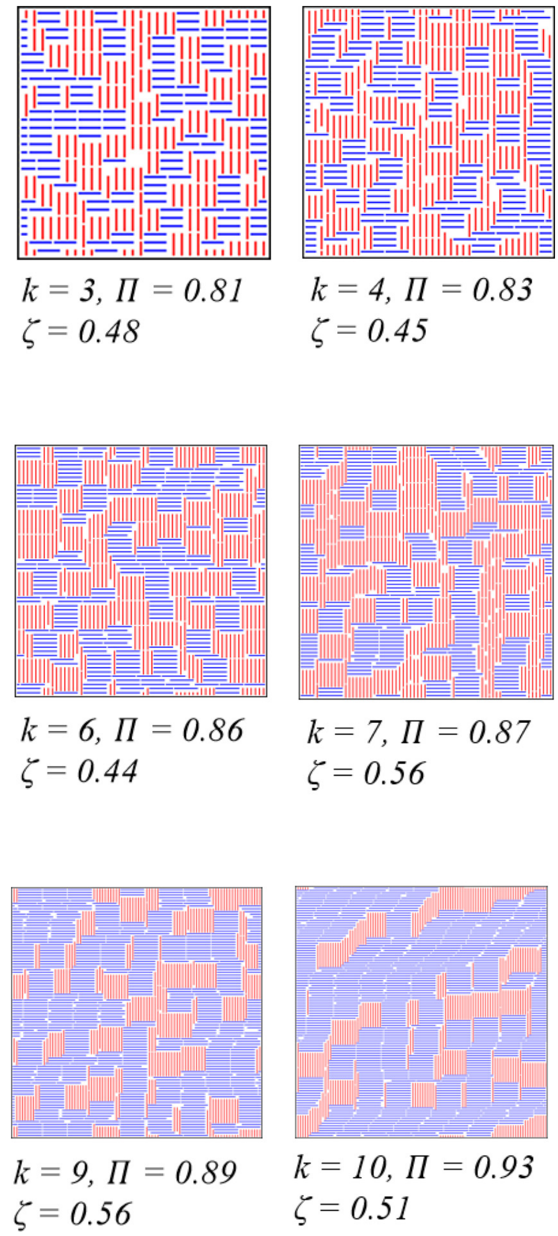

FIG. 8. Snapshots at concentration $\theta = 0.98$ for k values complementary to those reported in Fig. 7.

Values of parameter Π and for the corresponding mutability ζ (reported below) are given underneath along with the k value.

The nematic transition can be viewed as an ergodicity breakdown where the systems with rods over a minimum length and over a characteristic concentration prefer one specific dominant direction, making easier further depositions if they are parallel to the already existing majority. Other configurations including depositions with different orientations are no longer possible or extremely unlikely. This is not far from the ergodicity breakdown shown by magnetic systems over a minimum number of elements [81]. However, as the coverage continues to increase, individual behavior is lost in favor of group reorientations; then paths are obtained reaching a labyrinth-like configuration whose optimal organized goal would be something like the depositions presented in Fig. 2. As can be noticed from Fig. 8, the aspects of these high-coverage configurations are very similar to each other, independently of k. Moreover, parameter Π is near 0.9 for all these cases, thus pointing to the just mentioned optimal configuration depicted in Fig. 2.

Most of the previous figures reporting the concentration dependence of the parameters did not include error bars. The only exception was Fig. 4 due to its simplicity. This was due to two different reasons. First, error bars would overcrowd the most complex plots. Second, we will report now the

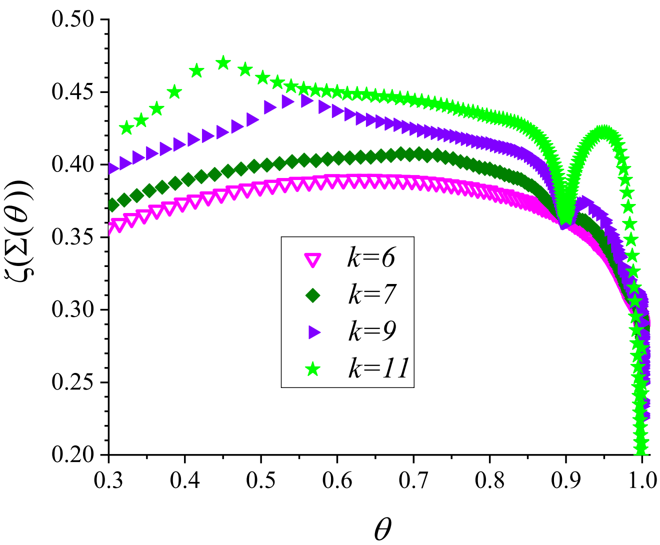

FIG. 9. Mutability for order parameter Σ, namely $\zeta(\Sigma(\theta))$, for $L/k = 10$ and different values of k.

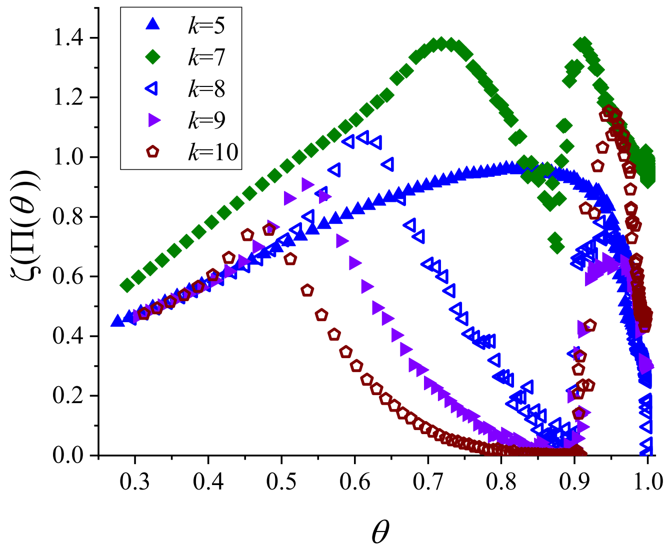

FIG. 10. Mutability of parameter Π, namely $\zeta(\Pi(\theta))$, for $L/k = 10$ and different values of k.

variability of the parameters using two alternative measures of this property: one is the Shannon entropy based on the static distribution of the data, the other is the mutability based on a dynamic measure of the information content of the data chain. As we report below, it turns out that the latter gives the better response to the variability of the data under analysis. Thus, mutability is a far better measure of variability than standard deviation or its related error bar analysis. However, Fig. 4 already indicates that error bars are larger precisely near the transition concentrations θ_1 and θ_2. This is also true for all the other figures where error bars were omitted.

We begin the information content analysis by presenting Fig. 9, where the mutability of the Σ function, namely $\zeta(\Sigma(\theta))$, is presented for selected values of k. The curve for $k = 6$ does not present any maximum and it is included as a reference, but curves for higher values of k present a structure that is progressively better defined as k increases.

It might be surprising that, in spite the parameter $\Sigma(\theta)$ itself not showing any indication of the transition at θ_1 and showing only a general response around θ_2, its mutability does maximize at these concentrations according to the k value. The maxima are broad but the mutability of the parameter indicates that a change of dynamics is present near the corresponding concentrations and follows the expected tendency as k increases.

Curves for $k \geqslant 7$ maximize around or over 0.92 corresponding to θ_2, in correspondence with the deviation from the linear behavior shown by the parameter itself, as \can be seen in the inset of Fig. 5. However, the characterization of this transition afforded by $\zeta(\Pi(\theta))$ allows a clearer determination of θ_2 as compared with the information provided by the parameter itself.

In Fig. 10 we present the mutability of parameter $\Pi(\theta)$ for selected values of k. The curve for $k = 5$ is included as a reference although it does not show a sharp maximizing structure. Similar curves are obtained for $k \leqslant 6$. Plots for $k \geqslant 7$ clearly recognize both θ_1 and θ_2 on the same footing. The critical concentrations are better defined than in any of the preceding determinations, with the parameter pointing to a clear interpretation of the phases present. The tendencies are also clear: θ_1 shifts to low concentration values while simultaneously θ_2 tends to high concentration values as k increases.

We have chosen mutability to do most of previous analysis, which is now justified by means of Fig. 11 for the case $k = 9$. Here parameter $\delta(\theta)$ is included as a reference. Three other curves are plotted: parameter $\Pi(\theta)$ itself, its mutability $\zeta(\Pi(\theta))$, and its Shannon entropy $H(\Pi(\theta))$. The transition at θ_1 is recognized by these three curves, with a clear advantage for $\zeta(\Pi(\theta))$ which shows the best defined maximum and sharper resolution. Then, for the second transition, $\delta(\theta)$ and $\Pi(\theta)$ move in different manners, crossing each other at θ_2. Near this value both $\zeta(\Pi(\theta))$ and $H(\Pi(\theta))$ maximize, with

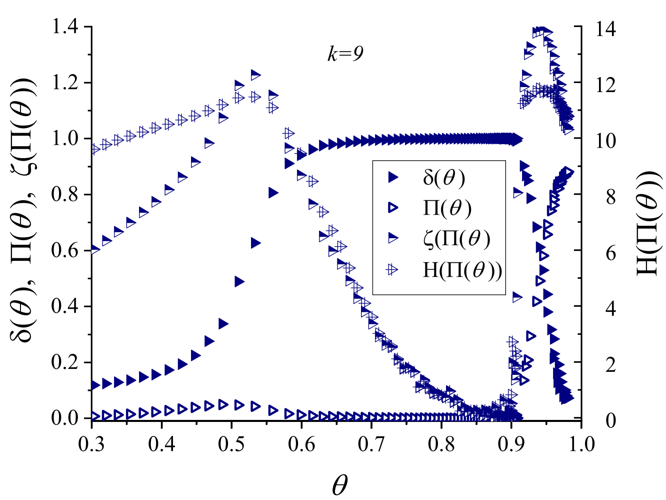

FIG. 11. Comparison of mutability and Shannon entropy of parameter $\Pi(\theta)$ for $k = 9$. In addition parameters Π and δ are also plotted to help in the discussion.

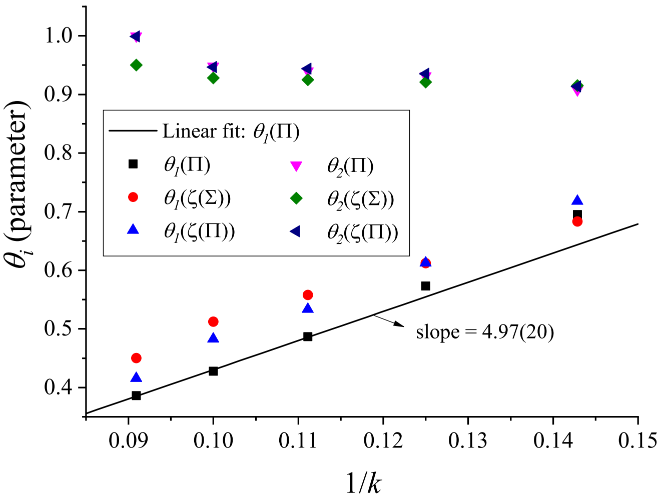

FIG. 12. Critical coverage values θ_i $(i = 1, 2)$ obtained by the different methods introduced in the present paper and $L/k = 10$. A linear fit for θ_1 obtained from the better defined parameter $\Pi(\theta)$ is also included.

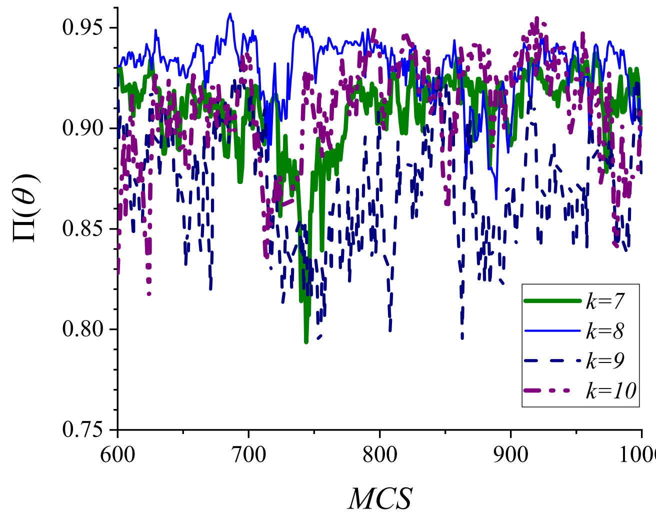

FIG. 13. A portion of the sequence for parameter Π at a concentration θ well over the second maximum θ_2 showing the oscillations present for high values of the chemical potential. Time is measured in MC steps (MCS) after equilibration.

the maximum being sharper the former one. Curves for other cases with $k \geqslant 7$ are similar to this one.

As can be observed, $\zeta(\Pi(\theta))$ and $H(\Pi(\theta))$ are somewhat related, a phenomenon that could deserve special attention but which is beyond the scope and goals of the present paper. The advantage shown by mutability over Shannon entropy has been also detected in other applications of these information recognizers [82].

Let us continue the analysis by considering the critical coverage values obtained from the use of the new parameters. From Fig. 5 we realize that the parameter Σ cannot produce any numerical indication of the critical coverage values at which the transitions take place. However, Fig. 6 shows that we can use the low-coverage maximum to define $\theta_1(\Pi)$. The definition of $\theta_2(\Pi)$ is somewhat trickier since this function was built to maximize at $\theta = 1$ regardless of the k value. So we define $\theta_2(\Pi)$ at the concentration where $\Pi(\theta) \approx 0.5$. Critical coverage values associated at the mutability values are directly obtained from the two maxima of each of the functions $\zeta(\Sigma(\theta))$ (see Fig. 9) and $\zeta(\Pi(\theta))$ (see Fig. 10).

These critical coverage values are plotted in Fig. 12. As can be seen, the tendencies are basically the same in spite of some minor differences among the methods. Generally speaking θ_1 tends to low values, eventually to zero. This is reinforced by the linear fit included for $\theta_1(\Pi)$ in Fig. 12, which is given by

$$\theta_1(k) = A + B\frac{1}{k} \qquad (k \geqslant 9), \tag{17}$$

where $A = -0.067(19)$ and $B = 4.97(20)$. Equation (17) is consistent with previous results obtained by Kundu and Rajesh [26], who reported that the critical density θ_1 follows a power law as $\theta_1(k) = Bk^{-1}$, with $B = 4.80(5)$. This expression was derived for large values of the k-mer size and lattice sizes in the thermodynamic limit ($L \to \infty$). The small deviation from 0 observed in A can be attributed to size effects (note that the calculations in Fig. 12 were done for $L/k = 10$).

On the other extreme θ_2 grows to eventually reach the value 1.0. However the high-coverage slow dynamics and its associated unstable behavior make difficult any further numerical treatment. So we can imagine that as the depositing k-mer tends to infinite length the nematic phase will be the only one present.

A careful look at the very high coverage values of the parameter $\Pi(\theta)$ in Figs. 4 and 6 may suggest that this parameter tends to unity as $\theta \to 1.0$. With the idea of elucidating this point we analyzed the time series for this parameter at these extreme coverage values after equilibration. In Fig. 13 we present a segment of the evolution of the parameter $\Pi(\theta)$ after equilibration; it is observed that $\Pi(\theta)$ oscillates strongly at high coverages. This is due to the dominant dynamics present at high coverages (large chemical potentials), which implies the shift of several rods at a time. It can also be noticed that the range of the oscillations for $\Pi(\theta)$ is larger for the higher values of k.

This behavior contrasts with the constant value close to 0.0 for $\Pi(\theta)$ present during the nematic phase. Moreover, the jump to recover high values shown in Figs. 4 and 6 is not reproducible in the sense that it occurs erratically depending on the trajectory of the attempts to change configurations established by the unstable dynamics present at high coverage. We have set a step counter to monitor the number of steps to obtain the first jump from the minimum value of $\Pi(\theta)$ to any value towards the monotonic tendency established in Fig. 6, thus initiating the "unfreezing" process of the nematic phase.

For values of k ranging from 7 to 11, we explored the minimum number of MCS to initiate the unfreezing process (this is a extremely time consuming task for the larger values of k). Results are presented in Fig. 14 as a function of k. It is quite clear that computer times necessary to handle this dynamics grow exponentially with the size of the depositing k-mer. This is the only reason we stopped at $k = 11$, whose results were extremely difficult to obtain and had large fluctuations. Actually, we were not able to unfreeze the nematic phase for $k = 12$ with the computer facilities at our disposal.

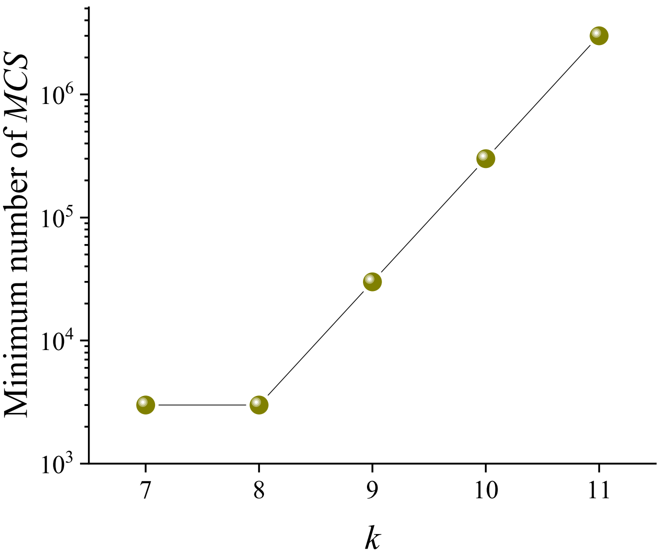

FIG. 14. Minimum number of MCS necessary to unfreeze the nematic phase at high θ values, versus the length of the depositing rod; $L/k = 10$.

IV. CONCLUSIONS

In the present paper the problem of excluded volume deposition of rigid rods of length k unit cells over square lattices is revisited. The following is a quick list of the main aspects considered here, which complement previous treatments of this very rich problem touching different aspects of statistical physics. (a) Differently than what three of us did in Ref. [36], we now use the improved algorithm defined in Ref. [32] which is now combined with information theory techniques. (b) Two new parameters (Π and Σ) are defined to better characterize the phases. (c) Mutability measurements done on these new parameters yield better precision on the critical coverage and more insight into the nature of the transitions. (d) Shannon entropy is used in this problem, which allows us to confirm previous critical behavior by an independent route. (e) The combination of the values of the new parameters, their mutability values, their Shannon entropy values, and snapshot analysis as coverage increases gives a more general and homogeneous picture valid for all k values. (f) This description allows us to propose that the triggering mechanism producing the nematic transition is an ergodic breakdown governed mainly by the value of k. We now review some of these aspects in more detail.

Two new short-distance complementary order parameters, Σ and Π, are introduced and discussed in relation to the ordered phases appearing in the system, particularly the high-coverage one characterized by path or labyrinth patterns. This is the phase at which the system arrives, regardless of the size k, which allows us to interpret the low-coverage nematic phase as an ergodicity breakdown present only when $k \geqslant 7$.

We found that parameter Σ is not able to evidence the nematic transition at θ_1. On the other hand, parameter Π evidences both the one at θ_1 and the high-coverage transition at θ_2. In contrast, the conventional order parameter δ does not indicate which phase is reached after the nematic phase disappears.

The size of the lattice L influences slightly the values of θ_1 and θ_2: they both move to higher concentrations as L grows for any given k. However, the tendencies are preserved, which allowed us to establish the numerical study based on systems sizes with $L/k = 10$.

In addition, the variabilities of the parameters were measured by two methods: mutability (dynamical information theory method) and Shannon entropy (static distribution analysis). The study showed that, although Σ showed no evidence of the nematic phase at θ_1, its mutability $\zeta(\Sigma(\theta))$ presents a maximum at these concentrations according to the k value. Regarding parameter Π both Shannon entropy and mutability are able to recognize transitions at θ_1 and θ_2, although the second is somewhat better defined.

Considering the critical coverage values θ_1 and θ_2 obtained from the new parameters and their mutabilities, we found a good agreement with previous results found in the literature. Generally speaking θ_1 tends to low values, eventually to zero, whereas θ_2 grows to eventually reach the value 1.0. However, the high-coverage slow dynamics and its associated unstable behavior make difficult any further numerical treatment. So we can imagine that the nematic phase will be the only one present when the depositing k-mer tends to infinite length.

Simulation dynamics at high coverage, is still very slow when we deal with large k-mers ($k > 10$). Changes involving groups of rows are progressively more difficult as coverage increases, leading to slower dynamics. This puts a limitation on the size k we can reach for these simulations ($k_{\max} = 11$).

Now the possibility is open to characterize k-mer depositions on other lattices using $\Pi(\theta)$ and $\zeta(\Pi(\theta))$ as the most appropriate parameters to detect the transitions associated with well defined phases. The limiting cases $k = 6$ and $k = 7$ could be also studied thoroughly by these parameters over a range of L values to better detect the borderline for the nematic phase. This is pointing towards a phase diagram for each lattice.

ACKNOWLEDGMENTS

This work was supported in part by CONICET (Argentina) under Project No. PIP 112-201101-00615; Universidad Nacional de San Luis (Argentina) under Project No. 03-0816; and the National Agency of Scientific and Technological Promotion (Argentina) under Project No. PICT-2013-1678. Partial support from the following Chilean sources is acknowledged: Fondecyt (Chile) under Contract No. 1190036, and Financiamiento Basal para Centros Científicos y Tecnológicos de Excelencia (Chile) through the Center for Development of Nanoscience and Nanotechnology (CEDENNA, Contract No. FB0807). All calculations were carried out using the supercomputing infrastructure of the NLHPC (ECM-02) at Centro de Excelencia en Modelación y Computación Científica at Universidad de La Frontera CEMCC-UFRO, Chile.

[1] L. Onsager, Ann. N.Y. Acad. Sci. **51**, 627 (1949).
[2] A. Verberkmoes and B. Nienhuis, Phys. Rev. Lett. **83**, 3986 (1999).
[3] A. Bellemans and R. K. Nigam, J. Chem. Phys. **46**, 2922 (1967).
[4] A. Bellemans and R. K. Nigam, Phys. Rev. Lett. **16**, 1038 (1966).
[5] F. H. Ree and D. A. Chesnut, J. Chem. Phys. **45**, 3983 (1966).
[6] K. Ramola and D. Dhar, Phys. Rev. E **86**, 031135 (2012).
[7] T. Nath, D. Dhar, and R. Rajesh, Europhys. Lett. **114**, 10003 (2016).
[8] T. Nath and R. Rajesh, J. Stat. Mech. (2016) 073203.
[9] D. Mandal, T. Nath, and R. Rajesh, J. Stat. Mech. (2017) 043201.
[10] P. W. Kasteleyn, Physica **27**, 1209 (1961).
[11] H. N. V. Temperley and M. E. Fisher, Philos. Mag. **6**, 1061 (1961).
[12] O. J. Heilmann and E. H. Lieb, Commun. Math. Phys. **25**, 190 (1972).
[13] D. A. Huse, W. Krauth, R. Moessner, and S. L. Sondhi, Phys. Rev. Lett. **91**, 167004 (2003).
[14] K. Ramola, K. Damle, and D. Dhar, Phys. Rev. Lett. **114**, 190601 (2015).
[15] D. Mandal and R. Rajesh, Phys. Rev. E **96**, 012140 (2017).
[16] P. Szabelski, W. Rżysko, T. Pańczyk, E. Ghijsens, K. Tahara, Y. Tobe, and S. De Feyter, RSC Adv. **3**, 25159 (2013).
[17] D. Ruth, R. Toral, D. Holz, J. Rickman, and J. Gunton, Thin Solid Films **597**, 188 (2015).
[18] D. Mandal, T. Nath, and R. Rajesh, Phys. Rev. E **97**, 032131 (2018).
[19] L. Mao, H. H. Harris, and K. J. Stine, J. Chem. Inf. Comput. Sci. **42**, 1179 (2002).
[20] B. C. Barnes, D. W. Siderius, and L. D. Gelb, Langmuir **25**, 6702 (2009).
[21] A. Ghosh and D. Dhar, Eur. Phys. Lett. **78**, 20003 (2007).
[22] D. A. Matoz-Fernandez, D. H. Linares, and A. J. Ramirez-Pastor, Eur. Phys. Lett. **82**, 50007 (2008).
[23] D. A. Matoz-Fernandez, D. H. Linares, and A. J. Ramirez-Pastor, Physica A **387**, 6513 (2008).
[24] D. A. Matoz-Fernandez, D. H. Linares, and A. J. Ramirez-Pastor, J. Chem. Phys. **128**, 214902 (2008).
[25] T. Fischer and R. L. C. Vink, Eur. Phys. Lett. **85**, 56003 (2009).
[26] J. Kundu and R. Rajesh, Phys. Rev. E **91**, 012105 (2015).
[27] P. Longone, D. H. Linares, and A. J. Ramirez-Pastor, J. Chem. Phys. **132**, 184701 (2010).
[28] P. Longone, M. Dávila, and A. J. Ramirez-Pastor, Phys. Rev. E **85**, 011136 (2012).
[29] P. Quiring, M. Klopotek, and M. Oettel, Phys. Rev. E **100**, 012707 (2019).
[30] D. H. Linares, F. Romá, and A. J. Ramirez-Pastor, J. Stat. Mech. (2008) P03013.
[31] J. Kundu, R. Rajesh, D. Dhar, and J. F. Stilck, in *Solid State Physics: Proceedings of the 56th DAE Solid State Physics Symposium 2011, 19–23 December 2011, SRM University, Kattankulathur, Tamilnadu, India*, edited by R. Mittal, A. K. Chauhan, and R. Mukhopadhyay, AIP Conf. Proc. No. 1447 (AIP, New York, 2012), p. 113.
[32] J. Kundu, R. Rajesh, D. Dhar, and J. F. Stilck, Phys. Rev. E **87**, 032103 (2013).
[33] M. Disertori and A. Giuliani, Commun. Math. Phys. **323**, 143 (2013).
[34] D. Dhar, R. Rajesh, and J. F. Stilck, Phys. Rev. E **84**, 011140 (2011).
[35] J. Kundu and R. Rajesh, Phys. Rev. E **88**, 012134 (2013).
[36] E. E. Vogel, G. Saravia, and A. J. Ramirez-Pastor, Phys. Rev. E **96**, 062133 (2017).
[37] J. Kundu and R. Rajesh, Phys. Rev. E **89**, 052124 (2014).
[38] T. Nath, J. Kundu, and R. Rajesh, J. Stat. Phys. **160**, 1173 (2015).
[39] P. Gurin, S. Varga, M. González-Pinto, Y. Martínez-Ratón, and E. Velasco, J. Chem. Phys. **146**, 134503 (2017).
[40] H. C. M. Fernandes, J. J. Arenzon, and Y. Levin, J. Chem. Phys. **126**, 114508 (2007).
[41] T. Nath and R. Rajesh, Phys. Rev. E **90**, 012120 (2014).
[42] R. J. Baxter, J. Phys. A **13**, L61 (1980).
[43] X. Wen, R. B. Meyer, and D. L. D. Caspar, Phys. Rev. Lett. **63**, 2760 (1989).
[44] S. Fraden, G. Maret, D. L. D. Caspar, and R. B. Meyer, Phys. Rev. Lett. **63**, 2068 (1989).
[45] P. G. De Gennes and J. Prost, *The Physics of Liquid Crystals* (Oxford University Press, Oxford, 1995).
[46] E. Grelet, Phys. Rev. Lett. **100**, 168301 (2008).
[47] Z. Dogic and S. Fraden, Phys. Rev. Lett. **78**, 2417 (1997).
[48] Z. Dogic and S. Fraden, Langmuir **16**, 7820 (2000).
[49] A. Kuijk, A. V. Blaaderen, and A. Imhof, J. Am. Chem. Soc. **133**, 2346 (2011).
[50] A. Kuijk, D. V. Byelov, A. V. Petukhov, A. V. Blaaderen, and A. Imhof, Faraday Discuss. **159**, 181 (2012).
[51] P. A. Buining and H. N. W. Lekkerkerker, J. Phys. Chem. **97**, 11510 (1993).
[52] M. P. B. van Bruggen, F. M. van der Kooij, and H. N. W. Lekkerkerker, J. Phys.: Condens. Matter **8**, 9451 (1996).
[53] A. Czogalla, D. J. Kauert, R. Seidel, P. Schwille, and E. P. Petrov, Nano Lett. **15**, 649 (2015).
[54] B. Dünweg, A. Milchev, and P. A. Rikvold, J. Chem. Phys. **94**, 3958 (1991).
[55] A. Patrykiejew, S. Sokołowski, and K. Binder, Surf. Sci. Rep. **37**, 207 (2000).
[56] S. J. Mitchell, G. Brown, and P. A. Rikvold, Surf. Sci. **471**, 125 (2001).
[57] J. P. Straley, Phys. Rev. A **4**, 675 (1971).
[58] D. Frenkel and R. Eppenga, Phys. Rev. A **31**, 1776 (1985).
[59] M. D. Khandkar and M. Barma, Phys. Rev. E **72**, 051717 (2005).
[60] R. L. C. Vink, Phys. Rev. Lett. **98**, 217801 (2007).
[61] E. A. DiMarzio, J. Chem. Phys. **35**, 658 (1961).
[62] M. Oettel, M. Klopotek, M. Dixit, E. Empting, T. Schilling, and H. Hansen-Goos, J. Chem. Phys. **145**, 074902 (2016).
[63] E. A. Guggenheim, Proc. R. Soc. London, Ser. A **183**, 203 (1944).
[64] E. E. Vogel, G. Saravia, F. Bachmann, B. Fierro, and J. Fischer, Physica A **388**, 4075 (2009).
[65] E. E. Vogel, G. Saravia, and L. V. Cortez, Physica A **391**, 1591 (2012).
[66] V. Cortez, G. Saravia, and E. E. Vogel, J. Magn. Magn. Mater. **372**, 173 (2014).
[67] E. E. Vogel and G. Saravia, Eur. Phys. J. B **87**, 177 (2014).
[68] E. E. Vogel, G. Saravia, J. Astete, J. Díaz, and F. Riadi, Physica A **424**, 372 (2015).
[69] D. J. Contreras, E. E. Vogel, G. Saravia, and B. Stockins, J. Am. Soc. Hypertens. **10**, 217 (2016).

[70] E. E. Vogel, G. Saravia, D. Pastén, and V. Muñoz, Tectonophysics **712**, 723 (2017).
[71] E. E. Vogel, G. Saravia, S. Kobe, R. Schumann, and R. Schuster, Renewable Energy **126**, 724 (2018).
[72] C. E. Shannon, Bell. Sys. Tech. J. **27**, 379 (1948).
[73] A. Crisanti, M. Falcioni, G. Paladin, M. Serva, and A. Vulpiani, Phys. Rev. E **50**, 138 (1994).
[74] H. Xi and J. D. Gunton, Phys. Rev. E **52**, 4963 (1995).
[75] R. V. Cakmur, D. A. Egolf, B. B. Plapp, and E. Bodenschatz, Phys. Rev. Lett. **79**, 1853 (1997).
[76] A. C.-L. Chian, R. A. Miranda, E. L. Rempel, Y. Saiki, and M. Yamada, Phys. Rev. Lett. **104**, 254102 (2010).
[77] R. A. Miranda, E. L. Rempel, and A. C.-L. Chian, Mon. Not. R. Astron. Soc. **448**, 804 (2015).
[78] P. Manshour, S. Saberi, M. Sahimi, J. Peinke, A. F. Pacheco, and M. R. Rahimi Tabar, Phys. Rev. Lett. **102**, 014101 (2009).
[79] N. Metropolis, A. W. Rosenbluth, M. N. Rosenbluth, A. H. Teller, and E. Teller, J. Chem. Phys. **21**, 1087 (1953).
[80] F. Y. Wu, Rev. Mod. Phys. **54**, 235 (1982).
[81] O. A. Negrete, P. Vargas, F. Peña, G. Saravia, and E. E. Vogel, Entropy **20**, 933 (2018).
[82] E. E. Vogel, F. G. Brevis, D. Pastén, V. Muñoz, R. Miranda, and A. Chian (unpublished).